IRAQI JOURNAL OF APPLIED PHYSICS
Vol. 22, No. 2, April-June 2026, pp. 281-288

Characterization and Antibacterial Activity of TeO_2-Reinforced PMMA–PS Nanocomposites Developed by Solution Casting Method

Montaser A. Mahdi [1*]
Zaid A. Hasan [2]
Khalid Al-Ammar [2]

[1] Ministry of Education, Director of Education, Babylon, IRAQ
[2] Department of Physics, College of Education for Pure Sciences, University of Babylon, Babylon, IRAQ
Corresponding author email: montaser.ahmad1988@gmail.com

The structural, morphological, and antibacterial properties of nanocomposites composed of a mixture of polymethyl methacrylate (PMMA) and polystyrene (PS) reinforced with tellurium oxide particles at 2%, 4%, and 6% by weight were studied in this research. It was proven that the solvent casting design was effective. The presence of bonds and interactions between the components of the nanocomposites was verified and the nanoparticles were well-distributed at low concentrations and aggregated at high concentrations. The presence and uniform distribution of tellurium and oxygen elements within the polymer matrix was confirmed, proving the successful incorporation of TeO_2 nanoparticles into the composite structure. The nanocomposite exhibited excellent activity against *Escherichia coli* and *Staphylococcus aureus* for antibacterial applications. The electrostatic interaction generates reactive oxygen species (ROS), leading to bacterial cell damage. All these results indicate that these compounds may have applications in the fields of medicine and antimicrobial packaging.

Keyword: Nanocomposites; Tellurium dioxide; Polymer blends; Antibacterial activity
Received: 30 July 2025; Revised: 22 October 2025; Accepted: 29 October; Published: 1 April 2026

1. Introduction

Advanced materials known as polymeric nanocomposites are created by mixing polymers with nanoparticles to enhance their properties. As the nanoparticles are distributed throughout a polymer matrix, they exhibit improved mechanical, thermal, electrical, and optical properties over the neat polymer, along with functionalisation, such as their antibacterial nature [1,2]. A larger surface area-to-volume ratio of nanoparticles in polymers improves their dispersibility, allowing the particles to be evenly distributed throughout the polymer [3,4].

Poly(methyl methacrylate) (PMMA) is a typical industrial polymer that is a member of the acrylic group. It stands out for its strength and heat resistance, as well as its comparatively high transparency of roughly 92% of visible light, which makes it a good glass substitute [5,6]. Furthermore, PMMA has mechanical qualities, including hardness and impact resistance, in addition to strong resistance to weather and to UV radiation [7,8]. These characteristics made it possible to produce windows, lit signs, optical lenses, dental and bone implants, as well as parts for automobiles and aircraft [9,10]. However, PMMA has several drawbacks. These include a low melting point compared to other polymeric materials, poor heat resistance, and vulnerability to organic solvents [11,12]. Because of these disadvantages, it can only be used in fields that don't need strong durability or chemical resistance.

In contrast, polystyrene (PS) is a well-known thermoplastic that is widely used due to its solid, transparent, and lightweight characteristics [13,14]. PS may be used for packing stores, plastic cups, computer disk containers, high insulation foam (cooler & sample case), and food packaging containers because it has good thermal and electrical insulation qualities and is water resistant [15,16]. PS, on the other hand, is a brittle substance with high flammability and low impact strength at low temperatures [17,18]. Polystyrene (PS) used in general applications is often modified to improve its properties through copolymerization or by adding additives.

The combination of PS and PMMA polymers offers a unique set of complementary physicochemical properties, which render them suitable host matrices for oxide nanoparticles such as TeO_2. PS imparts toughness, chemical inertness, and processability, whereas PMMA offers high optical transparency, mechanical stiffness, and thermal resistance. Partial miscibility of PMMA and PS enables phase morphology control, allowing PS domains to enhance nanoparticle dispersion by reducing polymer–nanoparticle interfacial tension. The ester and carbonyl groups of PMMA can also weakly interact with Te–O bonds via dipole–dipole or hydrogen bonding to enable smooth anchoring of TeO_2 nanoparticles on the matrix. Such synergistic interaction prevents agglomeration of the nanoparticles, improves mechanical toughness, and retains optical clarity. In return [19], these blends aim to reduce the limitations of each polymer and produce

a material with properties designed for more versatile applications. The modification of blends can be used not only to improve tensile strength and fracture properties (mechanical properties), but also to enhance the thermal and optical properties of the blend [20,21]. This amendment opens the door to new applications in fields that require a balance between transparency, durability, and ease of manufacturing. Tellurium oxide (TeO_2) is a metal oxide compound characterized by unique physical and chemical properties, making it an interesting material in the field of nanotechnology [22].

TeO_2 is known for its excellent optical properties, including a high refractive index and wide transparency across the electromagnetic spectrum, making it a promising candidate for optical and optoelectronic applications [23,24]. In addition, it has some unusual electrical properties. For example, in some of its crystalline forms, TeO_2 shows ionic conductivity, which means it could be used as a sensor or in electrochemical cells [25,26]. Recently, interest in tellurium oxide nanoparticles (TeO_2 NPs) has significantly increased due to their enhanced properties compared to bulk materials. Nanoparticles of tellurium oxide (TeO_2 NPs) exhibit dose-dependent antibacterial activity and have proven effective against a range of bacteria, including multidrug-resistant strains of *Escherichia coli*, such as MRSA (chromosomal polymyxin B resistance) and *Acinetobacter baumannii* [27,28]. Several things contribute to this antibacterial effect, including the production of reactive oxygen species (ROS). They attack bacterial cells using various tactics, such as disrupting the ability of bacterial enzymes to function and compromising the outer layer's permeability, which prevents the material from crossing. Shaking organelles can even have deleterious consequences on the contents of the cells themselves. When combined, these several methods killed the germs [29,30].

Additionally, the antimicrobial qualities of TeO_2 NPs offer them great potential as an antibacterial agent in the production of nanocomposite materials. Current industries, including food packaging, home goods, and antimicrobial textiles, may find usage for this. TeO_2 NPs can be introduced to polymer matrices without losing their effectiveness because of their fine chemical and thermal stability, according to reports [31]. TeO_2 NPs can be made using a variety of processes, such as pyrolysis, chemical precipitation, and wet chemical procedures. Each of these processes allows for exact control over particle size and shape to improve the desired characteristics [32,33]. Recent work has highlighted the antimicrobial potential of tellurium-based nanomaterials. Hesabizadeh et al. synthesized "naked" TeO_2 nanoparticles (~50–60 nm) by pulsed-laser ablation and reported significant inhibition of *E. coli* and *S. aureus* at low µg/mL concentrations, while demonstrating limited cytotoxicity *in vitro* [28]. Zhong et al. similarly observed dose-dependent antibacterial activity for TeO_2 sols [27]. Gupta et al. reported electrochemical evidence and antimicrobial assays that support ROS generation and membrane damage as key bactericidal mechanisms for TeO_2 [32]. Compared with these colloidal studies, embedding TeO_2 into PMMA–PS films (this work) reduces direct nanoparticle exposure but offers mechanical stability and re-usability; hence higher wt.% within the polymer matrix (2–6 wt.% in our films) are required to reach inhibition zones comparable to those reported for free nanoparticles. Finally, the observed bactericidal behavior is consistent with general metal-oxide mechanisms (ROS production, membrane disruption) reported for TiO_2 and ZnO systems [34,35].

2. Experimental Part

As shown in table (1) and Fig. (1), the materials used are polymers: PMMA, average Mw ~800000 g/mol, polystyrene (PS, average Mw ~250000 g/mol), tellurium oxide nanoparticles (TeO_2 NPs, average particle size 40–60nm), and chloroform (analytical grade) as a solvent.

The nanocomposites were prepared using a modified solution-casting method, as illustrated schematically in Fig. (1).

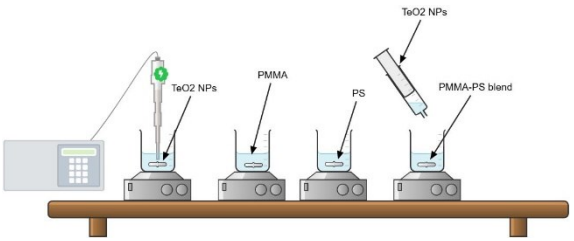

Fig. (1) Schematic diagram of preparation steps of PMMA-PS nanocomposites

The preparation process began with the preparation of a PMMA-PS polymer blend matrix. First, 0.8 g of polystyrene was dissolved in 30 mL of chloroform solution in a flask. The solution was then placed on a magnetic stirrer for one hour at room temperature to ensure complete dissolution and homogeneity. In parallel, 0.2 g of PMMA was dissolved in 30 ml of chloroform solution under continuous stirring for one hour at room temperature. The total weight of the polymer composite was 1 g. Immediately thereafter, the PS solution was gradually added to the PMMA solution under continuous stirring to prepare a PMMA: PS polymer matrix. After preparing the polymer matrix, TeO_2 NPs were incorporated at specific weight ratios of 2%, 4%, and 6% (calculated relative to the total polymer weight). To ensure optimal dispersion of the nanoparticles and prevent agglomeration within the polymer matrix.

The weight percentage of TeO_2 NPs in each nanocomposite was calculated using the following equation:

At 0.02g of TeO_2
Total remaining polymer weight = 1.00 − 0.02 = 0.98 g
1.00 − 0.02 = 0.98 g.

Because the ratio of PS to PMMA is 80:20, we calculate:
$m_{(PS)} = 0.98 \times 0.8 = 0.784$ g
$m_{(PMMA)} = 0.98 \times 0.2 = 0.196$ g

The same process for the rest of the addition ratios of TeO_2 NPs.

The solution was mixed alternately using a magnetic stirrer at a stirring speed and duration (500 rpm for 1 hour at room temperature) and then subjected to an ultrasonic probe for 2 hours. Before the casting process, substrates like Petri dishes were thoroughly cleaned and rinsed with ethanol and distilled water to ensure a surface suitable for film formation. PMMA-PS/TeO_2 nanocomposite thin films were fabricated using a direct casting technique onto these clean substrates. They were then left to dry completely at room temperature for 72 hours. To ensure complete removal of the solvent and the formation of solid, homogeneous films, the films were placed in a thermal oven at 50°C for 2 hours. After drying was complete, the PMMA-PS/TeO_2 nanocomposites were extracted from the Petri dishes, making them ready for various measurements and tests.

To investigate the produced nanocomposite's morphological and structural properties, several tests were conducted. A PANalytical X'Pert PRO diffractometer was used to acquire XRD data using Cu Kα-radiation (λ = 1.5406 Å) in the 2θ range of 10°-70°, with a step size of 0.02° and a counting duration of 1 s/step. Bruker Vertex 80 and Hyperion 2000 spectrometers were used to perform Fourier-transform infrared (FTIR) spectroscopy. The latter approach concentrates on TeO_2 NPs and polymer functional groups for production. If the spectrum indicates the integration of by-products, new chemical linkages can also be described. A field-emission scanning electron microscope (FE-SEM, TESCAN MIRA3) was used to introduce the surface morphology and surface topography of the PMMA–PS/TeO_2 nanocomposites at an accelerating voltage of 10-15 kV, with the specimen held at a distance of 8-10 mm. All images were captured using a secondary electron (SE) detector to provide high surface sensitivity and detailed topographical contrast. Finally, the antibacterial activities of the PMMA–PS/TeO_2 nanocomposites were evaluated using the agar well diffusion test against Mueller–Hinton agar. The inoculum density of bacteria was standardized to 0.5 McFarland standard. 6 mm diameter wells were filled with 50 µL of every dispersion of the nanocomposites (2, 4, and 6 wt.%). The plates were incubated at 37 °C for 24 h. For each experiment, triplicate sets were performed, and pure PMMA–PS was used as the negative control.

3. Results and Discussion

Figure (2) shows X-ray diffraction (XRD) patterns to validate the crystal structure of TeO_2 NPs, PMMA-PS blend and PMMA-PS/TeO_2 composite material. The 2θ values of TeO_2 and planes of widespread diffraction peaks were respectively 26.4°, 28.8°, 33.8°, 38.9°, 43.6°, 48.5°, 54.2°, 59.7°, 63.5°, and 68.2°, which are indexed to the (110), (101), (200), (210), (002), (220), (112), (202), (301), and (311) planes, respectively, as shown in Fig. (2a). The results are consistent with JCPDS card 03-065-2825 and previously published studies [32,36], while figure (2b) represents the XRD patterns for PMMA-PS blend and figures (2c, d and e) represent the XRD patterns for PMMA-PS/TeO_2 where the additional peaks observed in the XRD pattern could potentially be ascribed to the diffraction peaks originating from the polyethylene oxide (PS and PMMA) polymer. XRD results of the PMMA-PS composite with TeO_2 revealed significant changes in the positions of the peaks with increasing TeO_2 content. This change in position is due to the interaction between the TeO_2 nanoparticles and the polymer, which causes the peaks to deviate from their usual positions. This deviation can be explained by the structural effects resulting from the addition of TeO_2 to the polymer matrix, where the interlayer spacing of the TeO_2 crystals expands [37].

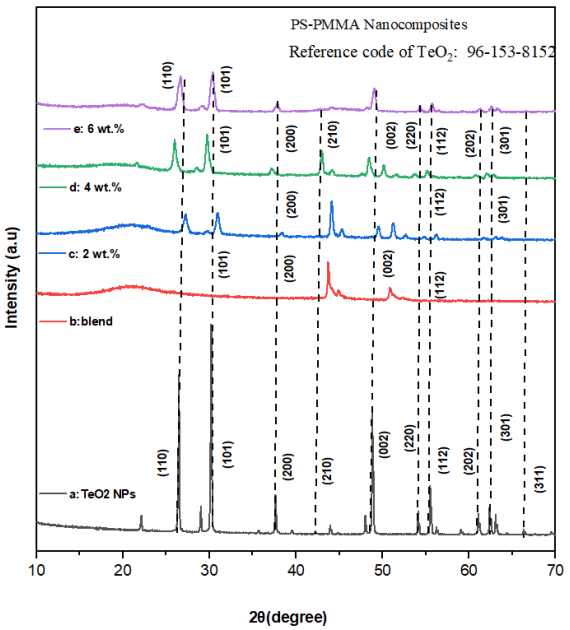

Fig. (2) XRD patterns of (a) TeO_2 NPs, (b) PMMA-PS blend, (c) 2, (d) 4, and (e) 6 wt.% of PMMA-PS/TeO_2 composite material

Figure (3) presents the FTIR spectra of PMMA–PS and PMMA–PS/TeO_2 nanocomposite films recorded in transmission mode at a resolution of 4 cm^{-1} with 32 scans in the range of 4000–610 cm^{-1}. The characteristic vibrational bands of PMMA and PS were clearly observed, and systematic spectral changes occurred upon TeO_2 incorporation at 2, 4, and 6 wt.%. The

resulting spectra exhibited a distinctive set of vibrational peaks. These active molecular patterns represent the chemical bonds within the polymer matrix, and the effects are due to the incorporation of nanoparticles. A specific, sharp and tall peak stands out across all frequencies when the weight ratio increases. In the range of 1723.35-1719.12 cm^{-1}, there was a distinct peak present in every sample, which was attributed to stretching vibrations of the carbonyl group (C=O stretch). This peak is characteristic of PMMA structure since it has an ester group.

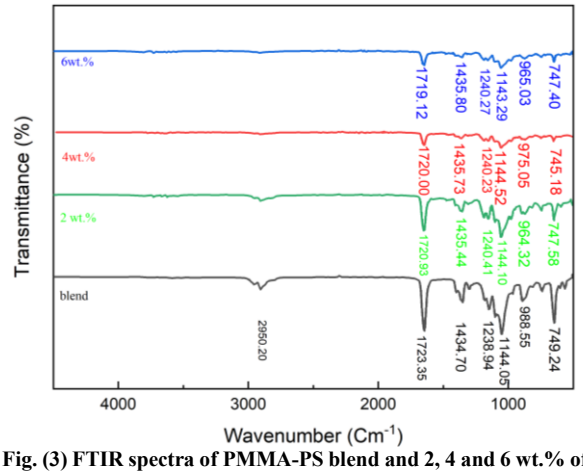

Fig. (3) FTIR spectra of PMMA-PS blend and 2, 4 and 6 wt.% of PMMA-PS/TeO_2 composite material

A slight change in the position of this peak was observed with variations in the TeO_2 ratio, indicating a limited change in the chemical environment surrounding the carbonyl group due to the interaction between the polymer blend and the nanoparticles. The peaks that appear in the range between 1434.70 and 1435.80 cm^{-1} are attributed to the bending of the methylene bond (bending $–CH_2$) or the vibrations of the aromatic ring in the PS polymer, indicating the presence of hydrocarbon chains in the polymer blend. Distinct peaks were also recorded in the range between 1238.94 and 1240.41 cm^{-1}, attributed to the stretching vibrations of C–O–C resulting from the ester groups in PMMA. This indicates the stability of this group and the lack of a significant effect on the addition of TeO_2. Peaks also appeared between 1143.29 and 1144.52 cm^{-1}, indicating additional vibrations associated with C–O bonds or bending vibrations of the -CH groups, which are often linked to the molecular structure of PMMA and PS. The lower-frequency region exhibited absorption maxima spanning from 964.32 to 988.55 cm^{-1}. These bands correspond to out-of-plane C–H bending modes typical of aromatic substituents in polystyrene and confirm that the polymer chains are adjusting to the surface of TeO_2 nanoparticles. A sequence of sharper bands from 800 to 610 cm^{-1}, corresponding to out-of-plane C–H bending, is another indication of the PS polymer and TeO_2 NPs [38]. The shifts in the FTIR bands with varying TeO_2 concentrations indicate an overlap and interaction between the added particles and the PMMA-PS functional groups, suggesting the formation of hydrogen bonds or physical/chemical interactions that affect the compound's molecular structure [39].

Figure (4) demonstrates the FE-SEM images of pure PMMA-PS and PMMA–PS/TeO_2 nanocomposites with various concentrations (2, 4, and 6) wt.% of TeO_2 NPs with a magnification of 120 KX and scale 500 nm. The homogeneous and uniform distribution of pure PMMA-PS in Fig. (4a) indicates a successful method for preparing the film. At 2 wt.% loading (Fig. 4b), the TeO_2 NPs were uniformly distributed within the polymer matrix, forming a continuous, well-dispersed nanonetwork. The absence of significant agglomeration suggests strong interfacial compatibility between the TeO_2 particles and the PMMA-PS copolymer. This structure is indicative of improved mechanical and optical properties, as previously reported in similar polymeric systems [39]. At 4 wt.% (Fig. 4c), slight nanoparticle aggregation began to appear, although the overall distribution remained relatively homogeneous. The particle sizes ranged from approximately 39 to 54 nm, which is typical for well-prepared metal oxide nanocomposites [40,41]. At 6 wt.% loading (Fig. 4d), more pronounced agglomeration was observed, with larger particle clusters (up to ~54 nm), leading to a rougher surface morphology and reduced dispersion uniformity. Such clustering is known to impair the mechanical integrity and optical clarity of nanocomposites, which aligns with findings from previous studies on TeO_2 and other metal oxide fillers [42,43]. FE-SEM micrographs were analysed using ImageJ software to determine the sizes of the nanoparticle clusters. At a 2% TeO_2 NPs concentration, the nanoparticles were evenly distributed (average size <100 nm). At a 4% concentration, small clusters with sizes of approximately 200–300 nm were observed, while at a 6% concentration, larger clusters (up to 600 nm) were formed.

Figure (5) shows the energy-dispersive X-ray spectroscopy (EDS) spectrum of the PMMA–PS/TeO_2 (4 wt.%) nanocomposite film, confirming the successful incorporation of TeO_2 NPs into the polymer matrix. The prominent peaks are carbon (C) and oxygen (O) from the PMMA–PS blend, with a characteristic tellurium (Te) signal easily detected at around 3.8 keV. Quantitative spectrum analysis yields ~91.2 at.% C (88.2 wt.%), 8.7 at.% O (11.3 wt.%), and 0.1 at.% Te (0.6 wt.%) as shown in table (2), as anticipated in view of the low overall content of the nanoparticles in the films (2–6 wt.% %). A weak but unambiguous Te signal further reinforces evidence for the incorporation of TeO_2 NPs by XRD and FTIR. Typical EDS response for low but detectable metal-oxide peaks in polymeric hosts has been reported before for analogous nanocomposites [44].

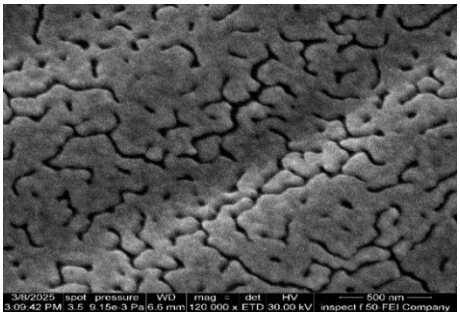

(a)

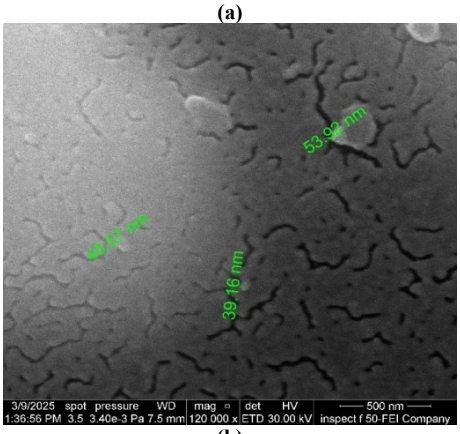

(b)

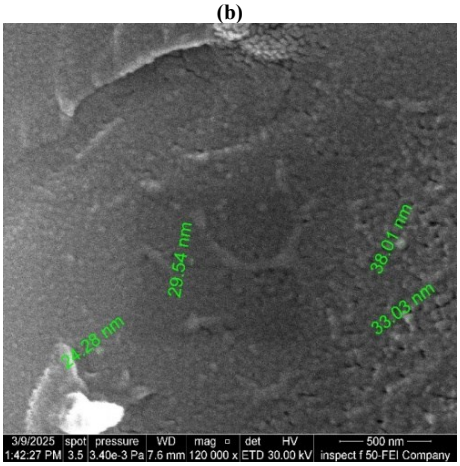

(c)

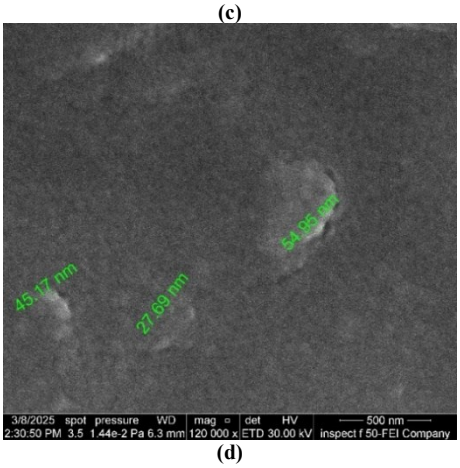

(d)

Fig. (4) FE-SEM images of PMMA-PS/TeO_2 nanocomposites, (a) for PMMA-PS, (b) 2 wt.% TeO_2 NPs, (c) 4 wt.% TeO_2 NPs, (d) 6 wt.% TeO_2 NPs

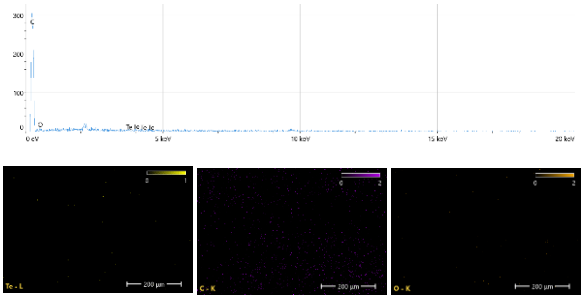

Fig. (5) EDS analysis of (a) PMMA-PS composites with 4 wt.% of TeO_2 NPs

Table (2) Quantitative EDS analysis showing the atomic and weight percentages of the detected elements

Element	Weight %	Atomic %
C	88.2	91.2
O	11.3	8.7
Te	0.6	0.1

4. Antibacterial Activity

Figure (6) shows the antibacterial activity of PMMA-PS\TeO_2 nanocomposites, evaluated by measuring the diameters of the clear inhibition zones around wells in plates inoculated with different bacterial strains. The results showed that TeO_2 is an effective antimicrobial agent against the tested microorganisms. *Escherichia coli* showed the highest level of resistance among the studied bacteria, with minimum inhibition zones of 12, 15, and 17 mm. *Staphylococcus aureus* has the least resistance, showing the largest area for inhibiting bacterial growth at 14, 18, and 21 mm. It is a Gram-positive bacterium. The illustrative figures in Fig. (5) and table (3) highlight the inhibition zones for both strains: (a) *Escherichia coli*, and (b) *Staphylococcus aureus*, which were obtained using the agar well diffusion method. Proteins, bacterial membranes, and nucleic acids are affected by the metal cations released by nanoparticles, which may cause structural changes and inhibit microbial proliferation [45,46]. Antibacterial activity of PMMA-PS/TeO_2 nanocomposites is attributed to several complementary mechanisms. The first mechanism involves an electostatic interaction between positively charged TeO_2 nanoparticles and negatively charged bacterial cell membranes, resulting in structural damage and increased membrane permeability [27,32]. Secondly, the generation of reactive oxygen species (ROS), such as hydroxyl radicals (OH_2), superoxide anions (O_2^-), and hydrogen peroxide (H_2O_2), leads to the oxidative degradation of essential biomolecules, including lipids, proteins, and nucleic acids, ultimately killing cells [47,48]. Thirdly, direct physical contact between nanoparticle assemblies and bacterial cell surfaces may create local mechanical stress and membrane disruption, decreasing cell viability ⁶. These mechanisms comply with previous research on TeO_2 and other metal

oxide nanoparticles (such as TiO_2 and ZnO) possessing similar antibacterial oxidative and electrostatic effects [49]. The synergistic inclusion of a stabilized PMMA–PS polymer matrix and reactive TeO_2 NPs thus provides nanocomposites with structural durability and strong antimicrobial activity.

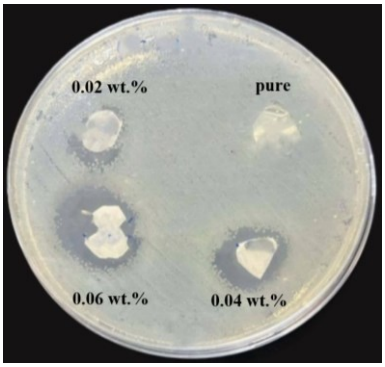

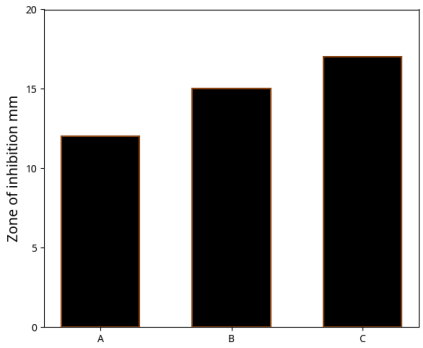

(a) *Escherichia coli*

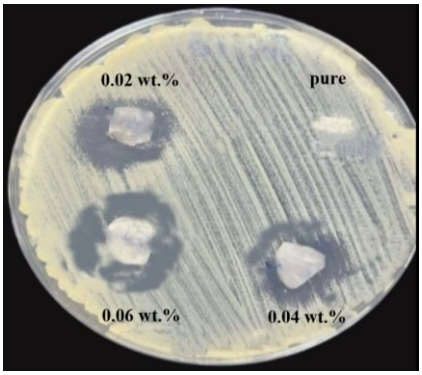

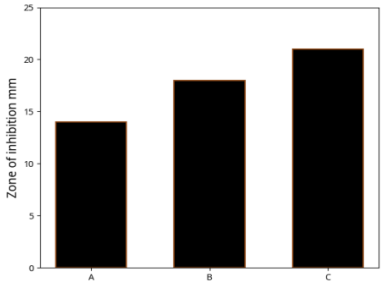

(b) *Staphylococcus aureus*

Fig. (6) Digital photographs and histograms for two types of bacteria

Table (3) Inhibition zone diameters (mm) of PMMA–PS/TeO_2 nanocomposites

Sample	*E. coli* (mm)	*S. aureus* (mm)
Pure PMMA–PS		
PMMA–PS/2 wt.% TeO_2	12 ± 0.5	14 ± 0.6
PMMA–PS/4 wt.% TeO_2	15 ± 0.7	18 ± 0.5
PMMA–PS/6 wt.% TeO_2	17 ± 0.6	21 ± 0.8

5. Conclusion

The successful incorporation of TeO_2 nanoparticles within the PMMA–PS matrix was confirmed and the crystallinity was increased with increasing nanoparticles loading. Strong polymer–nanoparticles interactions were indicated. Homogeneous nanoparticles dispersion at 2 wt.% was revealed, whereas small and larger agglomerates were observed at 4 and 6 wt.%, respectively. The presence and uniform distribution of Te and O elements within the composite were confirmed. Nanocomposites exhibited strong antibacterial activity with the largest inhibition zones for two different types of bacteria at 6 wt.% TeO_2 NPs, confirming their potential for antimicrobial and biomedical uses.

References

[1] S. Natarajan, S. Bajaj and R. Muniyappan, "Differences in antibacterial activity of PMMA/TiO_2/Ag nanocomposite on individual dominant bacterial isolates from packaged drinking water, and their consortium under UVC and dark conditions", *Appl. Surf. Sci*., 362 (2016) 93–101.

[2] E. Sharifzadeh et al., "A new approach in modelling of mechanical properties of nanocomposites: effect of interface region and random orientation", *Iran. Polym. J.,* 23(11) (2014) 835–845.

[3] M.A. Kadhim and E. Al-Bermany, "New fabricated PMMA–PVA/graphene oxide nanocomposites: Structure, optical properties and application", *J. Compos. Mater.,* 55(20) (2021) 2793–2806.

[4] H. Ahmed, H.M. Abduljalil and A. Hashim, "Novel studies on spectroscopic, optical and electronic properties of (PVA-TiO_2/SiC) nanocomposites for biological and optoelectronics applications", *Adv. Sci. Eng. Med.*, 11(6) (2019) 554–564.

[5] M.A. Kadhim and E. Al-Bermany, "Structural and DC-electrical properties of novel PMMA-PVA nanocomposites reinforced with graphene nanosheets", in *IOP Conf. Ser.: Mater. Sci. Eng.*, (2021) 12120.

[6] A. Emad and Z.A. Hasan, "Role of the Effect of Synthesis on Doping Mix Semiconductors Nanoparticles on Optical Properties of (PMMA) Polymer", *J. Nanostruct.*, 14(3) (2024) 818–830.

[7] N.N. Hafizah et al., "Bonding and mechanical

properties of PMMA/TiO_2 nanocomposites", *Adv. Mater. Res.*, 832 (2014) 700–705.
[8] G. Cascini and P. Rissone, "Plastics design: integrating TRIZ creativity and semantic knowledge portals", *J. Eng. Des.*, 15(4) (2004) 405–424.
[9] T.W. Clyne and D. Hull, **"An Introduction to Composite Materials**", Cambridge University Press (Cambridge, 2019).
[10] A.M. Díez-Pascual, "PMMA-based nanocomposites for odontology applications: a state-of-the-art", *Int. J. Mol. Sci.*, 23(18) (2022) 10288.
[11] D.W.K. Anti et al., "An overview of titanium dioxide effect on mechanical properties of PMMA-TiO_2 nanocomposites", *J. Int. Dent. Med. Res.*, 16(4) (2023) 1797–1803.
[12] M. Dai Prè et al., "Structural features, properties, and relaxations of PMMA-ZnO nanocomposite", *J. Mater. Sci.*, 50(5) (2015) 2218–2228.
[13] V. Syvänen, "Transfer of polystyrene micro-and nanoparticles across human placenta *ex vivo*", Ph.D. thesis, Itä-Suomen yliopisto (2024).
[14] E. Awodi and K.C. Adewumi, "Exploring the aesthetic applications of expanded polystyrene: an interdisciplinary review", *African J. Inter. Multidiscip. Stud.*, 6(1) (2024) 1–15.
[15] T. Arfin, F. Mohammad and N.A. Yusof, "Applications of polystyrene and its role as a base in industrial chemistry", *Polystyr. Synth. Charact. Appl. Nov. Sci. Publ.* (New York) (2015) 269–280.
[16] H.A.H. Slman and Z.A. Hasan, "Study addition of Fe_2O_3 Nanoparticles on Optical Properties for (PMMA-PS) Mixture", *IOP J. Phys.: Conf. Ser.*, (2021) 32100.
[17] W.H. Tesfamariam, **"Polystyrene Uses, Features, Production and Definition"**, (2024).
[18] A. Laachachi et al., "Effect of Al_2O_3 and TiO_2 nanoparticles and APP on thermal stability and flame retardance of PMMA", *Polym. Adv. Technol.*, 17(4) (2006) 327–334.
[19] G.A. AlZaidy, "Boosting of the optical properties, and electrical conductivity of polymethyl methacrylate (PMMA)/polystyrene (PS) blend with zinc oxide nanoparticles for high-performance energy storage devices", *J. Inorg. Organomet. Polym. Mater.*, 34(11) (2024) 5301–5312.
[20] C. Ton-That et al., "Effects of annealing on the5 surface composition and morphology of PS/PMMA blend", *Macromolecules*, 33(22) (2000) 8453–8459.
[21] S.S. Nemah and Z.A. Hasan, "Influence of Silver Nanoparticles on Optical Properties for (PS-PMMA) Blend", *J. Glob. Pharma Technol.*, 11(7) (2009) 325-330.
[22] A. Amari et al., "Electrochemical and optical properties of tellurium dioxide (TeO_2) nanoparticles", *Int. J. Electrochem. Sci.*, 16(2) (2021) 210235.
[23] V. Nagarajan and R. Chandiramouli, "TeO_2 nanostructures as a NO_2 sensor: DFT investigation", *Comput. Theor. Chem.*, 1049 (2014) 20–27.
[24] S.C. Cho, Y.C. Hong and H.S. Uhm, "TeO_2 nanoparticles synthesised by evaporation of tellurium in atmospheric microwave-plasma torch-flame", *Chem. Phys. Lett.*, 429(1-3) (2006) 214–218.
[25] S. Beke et al., "Characterisation of the ablation of TeO_2 crystals in air with femtosecond laser pulses", *J. Phys. D. Appl. Phys.*, 43(2) (2009) 25401.
[26] Y. Li et al., "Structural, electronic, and optical properties of α, β, and γ-TeO_2", *J. Appl. Phys.*, 107(9) (2010) 093506.
[27] C.L. Zhong et al., "Antioxidant and antimicrobial activity of tellurium dioxide nanoparticles sols", *J. Nano Res.*, 25 (2013) 8–15.
[28] T. Hesabizadeh et al., "Synthesis of 'naked' TeO_2 nanoparticles for biomedical applications", *ACS Omega*, 7(27) (2022) 23685–23694.
[29] K.R. Raksha, S. Ananda and N.M. Madegowda, "Study of kinetics of photocatalysis, bacterial inactivation and OH scavenging activity of electrochemically synthesised Se^{4+} doped ZnS nanoparticles", *J. Mol. Catal. A Chem.*, 396 (2015) 319–327.
[30] R. Tankhiwale and S.K. Bajpai, "Preparation, characterisation and antibacterial applications of ZnO-nanoparticles coated polyethylene films for food packaging", *Colloids Surf. B Biointerfaces*, 90 (2012) 16–20.
[31] A. Singh et al., "TeO_2 deposited ZnO nanotubes combined with cefotaxime as a nanoantibiotic against *Klebsiella pneumoniae*", *Mater. Today Proc.*, 67 (2022) 451–455.
[32] P.K. Gupta et al., "Electrochemical and antimicrobial activity of tellurium oxide nanoparticles", *Mater. Sci. Eng. B*, 211 (2016) 166–172.
[33] T. Siciliano et al., "Porous tellurium oxide microtubes for room-temperature NO_2 gas sensors", *Sens. Actuat. B Chem.*, 201 (2014) 138–143.
[34] D.A. Serov et al., "Review of antimicrobial properties of titanium dioxide nanoparticles", *Int. J. Mol. Sci.*, 25(19) (2024) 10519.
[35] N. Ranjbar-Jamalabadi et al., "Antimicrobial feature of nanoparticles in the antibiotic resistance era: from mechanism to application", *Adv. Biomed. Res.*, 13(1) (2024) 113.
[36] I.M. Mustapha et al., "The role of ZnO in TeO_2 thin films for optical and radiation dosimetry applications", *Heliyon*, 11(4) (2025) e42664.

[37] S. Kuzeci et al., "Free-volume analysis of the structural and dielectric properties of PMMA/TeO_2 composites via positron annihilation lifetime spectroscopy", *J. Alloys Compd.*, 1004 (2024) 175938.
[38] E. Mansour, "FTIR spectra of pseudo-binary sodium borate glasses containing TeO_2", *J. Mol. Struct.*, 1014 (2012) 1–6.
[39] I.H. Dwirekso, M. Ibadurrohman and T. Elysabeth, "The Effect of Morphology on Antibacterial Properties of CuO-Doped TiO_2-SiO_2 Nanocomposites", *J. Eng. Sci. Technol.*, 17(3) (2022) 1820–1832.
[40] Z. Li, "Synthesis and characterisation of conducting polymer nanostructures and their application in sensors", Ph.D. thesis, Missouri University of Science and Technology (2010).
[41] F.H. Oraibi et al., "(PS-PMMA-ZnO) nanocomposites fabrication and investigation their electrical properties for piezoelectric application", in *E3S Web of Conf.*, EDP Sciences, (2024) 7010.
[42] F.M. Nayef and B.H. Rabee, "Study the Optical and Morphological Properties of (PMMA/PS/Al_2O_3) Nanocomposites Before and After Exposed to Argon Plasma: Study PMMA/PS/Al_2O_3 Nanocomposites Before and After Argon Plasma Impact", *J. Kufa-Phys.*, 15(02) (2023) 62–85.
[43] A.J. Haider et al., "Impact of PS/PMMA polymer ratios with nanocomposite material on optical and morphological properties", *Ziggurat J. Mater. Technol.*, 1(1) (2020) 23–32.
[44] D. Debnath and B.B. Khatua, "Preparation by suspension polymerisation and characterisation of polystyrene (PS)-poly (methyl methacrylate) (PMMA) core-shell nanocomposites", *Macromol. Res.*, 19(6) (2011) 519–527.
[45] W.K. Khalef, T.R. Marzoog and A.D. Faisal, "Synthesis and characterisation of tellurium oxide nanoparticles using pulse laser ablation and study their antibacterial activity", in *IOP J. Phys.: Conf. Ser.*, (2021) 12049.
[46] S. Ramesh et al., "Rod-like structure of cotton cellulose/polyvinyl alcohol/tellurium dioxide (TeO_2) hybrid nanocomposite and antimicrobial properties", *Polym. Plast. Technol. Eng.*, 57(11) (2018) 1131–1138.
[47] K.R. Raghupathi, R.T. Koodali and A.C. Manna, "Size-dependent bacterial growth inhibition and mechanism of antibacterial activity of zinc oxide nanoparticles", *Langmuir*, 27(7) (2011) 4020–4028.
[48] V. Lakshmi Prasanna and R. Vijayaraghavan, "Insight into the mechanism of antibacterial activity of ZnO: surface defects mediated reactive oxygen species even in the dark", *Langmuir*, 31(33) (2015) 9155–9162.
[49] M.C. Zambonino et al., "Green synthesis of selenium and tellurium nanoparticles: current trends, biological properties and biomedical applications", *Int. J. Mol. Sci.*, 22(3) (2021) 989.

Table (1) Synthesis conditions of samples

Sample	$m_{(PS)}$ (g)	$m_{(PMMA)}$ (g)	TeO_2 Concentration (wt. %)	Sonication Time (h)	Mixing Time (h)	Drying Method
PMMA-PS	0.200	0.800	0	2	1	72 h at R.T. then in a thermal oven at 50°C for 2 hours
PMMA-PS\TeO_2	0.196	0.784	2	2	1	
PMMA-PS\TeO_2	0.192	0.768	4	2	1	
PMMA-PS\TeO_2	0.188	0.752	6	2	1	

